J. Fluid Mech. (1981), *vol.* 107, *pp.* 89–107
Printed in Great Britain

Numerical solutions for the compressible flow in a rapidly rotating cylinder

By G. J. DICKINSON
Technical Department, BNFL, Capenhurst Works, Chester CH1 6ER
AND I. P. JONES
Computer Science and Systems Division, A.E.R.E. Harwell, Didcot, Oxon OX11 ORA

(Received 20 July 1979 and in revised form 16 April 1980)

Numerical results are presented for the flow field in a rapidly rotating gas. These results are compared with the predictions of asymptotic theories, particularly those of Brouwers concerning viscous effects. The comparison shows that the effect of the viscous core is important and the extent of the different flow regimes is well predicted by the theory of Brouwers.

1. Introduction

In recent years considerable theoretical effort has been devoted to the problem of compressible flow in a cylinder rotating rapidly about its axis. The primary motivation for this work is to obtain an understanding of the flow field in a gas centrifuge used in the separation of the isotopes of uranium. The problem is, however, intrinsically interesting in its own right from the viewpoints of both analytical and numerical approaches.

For uniform temperatures and no external perturbations the flow pattern is given by rigid body rotation. Departures from rigid body rotation are created as a result of deviations in the boundary conditions on the surface of the cylinder and the end walls, for example, by differential rotation of the end walls. A considerable simplification of the problem is obtained by assuming that departures from rigid body rotation are small. The governing flow equations may then be linearized about rigid body motion.

One approach to the solution of these linearized equations was originally developed for the case of a semi-infinite cylinder by Steenbeck (1958) and Parker & Mayo (1963), and has been termed the long-bowl approach. Viscous forces are assumed to be important everywhere, with the consequence that any axial velocity profile established by the boundary conditions on the cylinder end walls decays axially. The solution may then be expanded in a series of decaying exponentials, e.g.

$$q_z^* = \sum_i f_i(r^*)\, e^{-\lambda_i z^*}$$

where q_z^* is the axial velocity, r^* the radial distance from the axis and z^* the distance from the end wall. This gives rise to an eigenvalue problem for the unknown decay rates λ_i. For certain parameter values, particularly for high peripheral velocities and low pressures these decay rates are quite large and the magnitude of the axial velocity decreases very quickly away from the end walls.

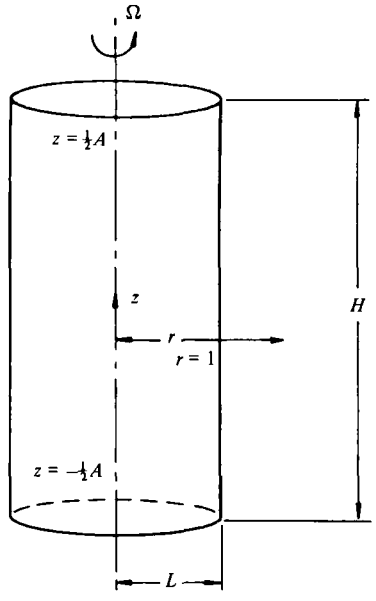

FIGURE 1. Geometrical configuration.

A second approach is based upon the asymptotic expansions used by Stewartson (1957) for the incompressible case. With this approach it is assumed that the Ekman number E, the ratio of viscous forces to rotational forces, is small. Consequently viscous forces are important only in boundary layers near the end walls, cylinder wall and in any shear layers present. Elsewhere the flow is effectively inviscid, leading to a non-decaying flow profile in the centre of the cylinder. That is, the axial velocity outside the boundary layers depends only upon the radius and is independent of the distance from the end walls. An Ekman boundary layer of thickness order $E^{\frac{1}{2}}$ is found on each of the cylinder end walls and drives the axial flow in the interior. This axial flow is rechannelled around the cylinder in boundary layers on the side walls of thickness order $E^{\frac{1}{3}}$ and $E^{\frac{1}{4}}$, the Stewartson $E^{\frac{1}{3}}$ and $E^{\frac{1}{4}}$ layers. For antisymmetric boundary conditions the $E^{\frac{1}{4}}$ layer is not needed and only the $E^{\frac{1}{3}}$ layer is present. This approach has been generalized to compressible flow by, among others, Sakurai & Matsuda (1974), Nakayama & Usui (1974) and Durivault & Louvet (1976). It is often referred to as the modified incompressible or 'short-bowl' approach. Summaries of both these approaches and extensive bibliographies are given by Rätz (1978) and Soubbaramayer (1979).

The first approach leads to solutions which may have considerable axial decay, whereas the second leads to solutions with no axial decay. However the modified incompressible approach depends on the assumption that viscous forces are small away from boundaries and shear layers. At high rotational speeds the density near the axis of rotation becomes extremely low. Hence the kinematic viscosity, μ/ρ, where μ is the dynamic viscosity and ρ is the density, becomes large with the result that viscous forces are important once more. The region where these viscous forces are important is known as the viscous core. Using scaling arguments Brouwers (1976, 1978*b*) has deduced the parameter ranges where the viscous core is non-existent, leading to short bowl solutions, and where the core extends over the entire cylinder giving axial decay and long bowl solutions. In between there exists both a viscous core and an inviscid

non-decaying region with the usual viscous boundary layers near the rigid walls. Brouwers (1978*a*) has also used approximate Pohlhausen techniques to obtain solutions for the side-wall boundary layer and the viscous core layer. These solutions allow a more precise estimate for the position of the viscous core and side wall boundary layer for antisymmetric boundary conditions.

The primary purpose of this paper is to investigate the results of Brouwers concerning the range of validity of the short bowl regime. In § 2 the numerical solution technique is briefly described, particularly the techniques used for resolving the boundary layers. In § 3, a detailed comparison between the numerical results and asymptotic predictions from Brouwers' theories is carried out for two simple model sets of antisymmetric boundary conditions. These are a simple 'friction' drive and a linear 'thermal' drive. The primary conclusion to be drawn from these results is that the predictions of Brouwers are in broad agreement with the numerical results and provide a unified framework for the solution of the linearized equations.

2. Mathematical and numerical formulation

Consider a gas uniformly rotating with angular velocity Ω in a cylinder of height H and radius L as shown in figure 1. For a uniform temperature $T^* = T_0^*$ the system is described by rigid body rotation:

$$\left.\begin{aligned} \mathbf{q}^* = 0, \quad \rho_B^* = \rho_w^* \exp \frac{M\Omega^2}{2RT_0^*}(r^{*2} - L^2), \\ T^* = T_0^*, \quad p_B^* = \frac{RT_0^*}{M}\rho_B^*, \end{aligned}\right\} \tag{2.1}$$

where $\mathbf{q}^*$ is the velocity relative to the rigid body motion, ρ_B^* the density, ρ_w^* the cylinder wall density, r^* the radial distance from the axis of rotation, M the molecular weight of the gas, R the gas constant and p_B^* the pressure. A small perturbation applied to the system induces a flow within the cylinder. This perturbation is defined by a Rossby number δ. For example, if the angular velocity is perturbed by a small angular velocity $\pm \frac{1}{2}\Delta\Omega$ on the end walls the Rossby number is $\Delta\Omega/\Omega$. Similarly for temperature perturbations $\pm \frac{1}{2}\Delta T^*$, $\delta = \Delta T^*/T_0^*$. For a small Rossby number, δ, the solution may be expanded as a Taylor series in δ about rigid-body motion. The linearized equations are obtained by ignoring terms of $O(\delta^2)$ and assuming axisymmetric perturbations. The approach and notation used to obtain the linear equations is similar to that used by Matsuda, Hashimoto & Takeda (1976).

Non-dimensional cylindrical co-ordinates r, θ, z are defined by

$$(r, \theta, z) = (r^*, \theta, z^*)/L$$

and non-dimensional variables as

$$(u, v, w) = (q_r^*, q_\theta^*, q_z^*)/L\Omega\delta, \quad T = (T^* - T_0^*)/T_0^*\delta, \quad p = (p^* - p_B^*)/p_B^*\delta,$$

where

$$p_B^* = \frac{RT_0^*}{M}\rho_B^*, \quad \rho_B^* = \rho_w^* \exp[\tfrac{1}{2}G(r^2 - 1)], \quad G = \frac{M\Omega^2 L^2}{RT_0^*}.$$

The subscript B refers to the unperturbed 'basic' flow and the subscript w to quantities evaluated at the cylindrical wall.

The equations may then be expressed as:

continuity,
$$\frac{\partial}{\partial r}(\epsilon_B ru)+\frac{\partial}{\partial z}(r\epsilon_B w)=0; \tag{2.2}$$

r momentum,
$$-2v+\frac{1}{G}\frac{\partial p}{\partial r}+rT=\frac{E}{\epsilon_B}\left\{\frac{\partial}{\partial r}\frac{1}{r}\frac{\partial}{\partial r}(ru)+\frac{\partial^2 u}{\partial z^2}+\frac{1}{3}\frac{\partial}{\partial r}\left\{\frac{1}{r}\frac{\partial}{\partial r}(ru)+\frac{\partial w}{\partial z}\right\}\right\}; \tag{2.3}$$

θ momentum,
$$2u=\frac{E}{\epsilon_B}\left\{\frac{\partial}{\partial r}\frac{1}{r}\frac{\partial}{\partial r}(rv)+\frac{\partial^2 v}{\partial z^2}\right\}; \tag{2.4}$$

z momentum,
$$\frac{1}{G}\frac{\partial p}{\partial z}=\frac{E}{\epsilon_B}\left\{\frac{1}{r}\frac{\partial}{\partial r}\left(r\frac{\partial w}{\partial r}\right)+\frac{\partial^2 w}{\partial z^2}+\frac{1}{3}\frac{\partial}{\partial z}\left\{\frac{1}{r}\frac{\partial}{\partial r}(ru)+\frac{\partial w}{\partial z}\right\}\right\}; \tag{2.5}$$

and energy,
$$-ruP_rG\left(\frac{\gamma-1}{\gamma}\right)=\frac{E}{\epsilon_B}\left(\frac{1}{r}\frac{\partial}{\partial r}\left(r\frac{\partial T}{\partial r}\right)+\frac{\partial^2 T}{\partial z^2}\right). \tag{2.6}$$

In the above
$$\epsilon_B=\exp\left[\tfrac{1}{2}G(r^2-1)\right] \tag{2.7}$$

and
$$\nabla.\mathbf{u}=\frac{1}{r}\frac{\partial}{\partial r}(ru)+\frac{\partial w}{\partial z}. \tag{2.8}$$

The equation of state then becomes an equation for the density perturbation ρ

$$p=\rho+T.$$

The solutions of these linearized equations are governed by the four non-dimensional parameters, G, the speed parameter, $E=\mu/\Omega L^2\rho_w^*$, the Ekman number, $P_r(\gamma-1)/\gamma$, a thermodynamic parameter, $A=H/L$, the aspect ratio; P_r is the Prandtl number, $\mu C_p/k$, C_p and C_v are the specific heats of the gas at constant pressure and volume respectively, γ is their ratio and k is the thermal conductivity. These parameters may be combined to give the Brinkman number

$$Br=\frac{\mu\Omega^2L^2}{kT_0^*}=GP_r(\gamma-1)/\gamma,$$

the modified Ekman number, $E^*=\frac{1}{4}EG^2$, and the modified aspect ratio $A^*=\frac{1}{2}AG$, Brouwers (1978*b*).

The program PACE (Program for the Axisymmetric Centrifuge Equations), used to obtain the present numerical results, solves the 'primitive variable' form of the finite difference equations, i.e. it solves a finite difference representation of (2.2)–(2.6) for the velocities, pressure and temperature.

In the present problem the boundary layers are extremely small when compared to the overall cylinder dimensions. In order to achieve an accurate numerical solution it is essential that the grid be chosen so that the boundary layers are resolved. Many conventional finite difference schemes using variable grids are only first-order accurate and to prevent gross errors from using a highly stretched grid it is customary to limit the 'mesh expansion ratio'. Typical values for this expansion ratio are about 1·1. The requirement to resolve the boundary layers for such mesh expansion ratios implies an enormous number of mesh points with consequential implications on program size and execution time.

In the program PACE the finite difference mesh is chosen by a smooth stretching function, with equally spaced intervals in the stretched function. The resulting

equations are now second order accurate in the stretched function. This technique is discussed in detail by Kálnay de Rivas (1972). It should be emphasized that the stretching function is used only to obtain the mesh; the resulting finite difference equations being similar to those found when using more conventional differencing techniques. The stretching functions used are similar to those described by Orsag & Israeli (1974) and may also be used to resolve interior shear layers. Using this technique, mesh expansion ratios of 5 and more are quite common and, as will be seen, the resolution of the boundary layers is very good.

As is customary with the primitive variable formulation the program uses a staggered grid system with the variables defined at different spatial locations (Roache 1972). To avoid difficulties in calculating the pressure a block iterative method has been adopted for the solution of the finite difference equations. The computational domain is divided into several overlapping blocks. The iterative technique cycles around each block sequentially solving the equations within each block by a direct method. The direct method used is a general sparse matrix linear equation solver, MA28A, from the Harwell Subroutine Library (Duff 1977). This technique effectively overcomes bandwidth limitations found when using a direct method on the full set of finite difference equations. It also enables efficient use to be made of backing store since only one block need be in core at any one time.

For all the results presented here, the thermodynamic parameter $P_r(\gamma-1)/\gamma$ has been taken to be 0·06. Most of the results have been obtained with 15 intervals in the radial direction and 24 intervals in the axial direction, although some have been repeated with double the resolution in both directions. An inner boundary has been assumed at $r = 0{\cdot}1$ with $u = 0$, $v = 0$, $\partial w/\partial r = 0$ and $\partial T/\partial r = 0$ at $r = 0{\cdot}1$. Due to the large change in density across the machine however, the solutions in the main body of the flow are insensitive to the exact location of this inner boundary and to the exact form of the boundary conditions.

3. Results: antisymmetric boundary conditions

In this section results for antisymmetric boundary conditions are considered. When the boundary conditions are antisymmetric the asymptotic analysis is simplified and for the numerical approach, the finite difference equations need only be solved for half the cylinder, considerably reducing the time required for computation.

Two simple model boundary conditions are studied. The first has rigid end walls rotating slowly relative to the wall of the cylinder with constant angular velocity perturbations $\mp \frac{1}{2}\Delta\Omega$, i.e.

$$v = -\tfrac{1}{2}r, \quad z = \tfrac{1}{2}A;$$

$$v = \tfrac{1}{2}r, \quad z = -\tfrac{1}{2}A.$$

This is referred to as friction drive. The asymptotic analysis of Brouwers (1978*b*) shows that, for the parameter ranges considered here, the equations may be expressed in terms of a stream function and a quantity $\chi = v/r - \frac{1}{2}T$, only. This implies that similar effects to the friction drive are induced by imposing temperatures $T = \pm 1$ on the end walls with the cylinder wall remaining at $T = 0$. Numerical computations have been performed for both cases, the numerical values of the stream function being found to be identical to at least two significant figures.

The second has a temperature perturbation $\pm \frac{1}{2}\Delta T^*$ on the end walls with a linear temperature profile on the cylinder wall, i.e.

$$T = \tfrac{1}{2}, \qquad z = \tfrac{1}{2}A;$$
$$T = -\tfrac{1}{2}, \qquad z = -\tfrac{1}{2}A;$$
$$T = z/A, \quad r = 1.$$

(a) *Friction drive*

The modified incompressible, or short-bowl regime, has a non-decaying inviscid flow in the centre of the cylinder which is induced by the motion generated in the end-wall Ekman boundary layers by the imposed boundary conditions, the 'Ekman suction'. The thickness of the Ekman layer is order $E^{\frac{1}{2}}$. The inviscid flow is rechannelled around the cylinder in a boundary layer associated with the cylinder wall, known as the Stewartson layer. This layer has a thickness of order $E^{\frac{1}{3}}$. When the density becomes sufficiently small towards the axis, Brouwers postulates that diffusive effects are again important, giving a viscous core. For certain parameter values the viscous core meets the cylinder wall Stewartson layer and viscous effects become important everywhere. This gives rise to the long-bowl regime where the flow is governed by eigenfunctions which decay from the end walls.

Using scaling arguments Brouwers (1976, 1978*b*) gives order of magnitude estimates for the extent of the viscous Stewartson layer and the viscous core in terms of the parameter x, defined by

$$x = \tfrac{1}{2}G(1-r^2).$$

The Stewartson layer/inviscid region boundary, x_s, is given by $x_s \sim G(AE)^{\frac{1}{3}}$, and the inviscid region/viscous core boundary, x_c, by $x_c \sim \ln(EG^3A)^{-1}$. The changeover from the short bowl regime to the long bowl regime therefore occurs when $x_c = x_s$. Brouwers (1976, 1978*b*) obtained a series solution for the Stewartson layer equations (under the assumption that $e^x \sim 1$ in the Stewartson layer) but was unable to obtain an analytic solution for the viscous core equations. Based on these calculations he could only give order of magnitude estimates as to the parameter values where a well-defined inviscid region occurs.

Using an approximate solution technique however for the Stewartson $E^{\frac{1}{3}}$ layer and viscous core equations Brouwers (1978*a*) predicted at the mid-plane of the cylinder, $z = 0$

$$x_s = 2{\cdot}07G(AE)^{\frac{1}{3}}(1+\tfrac{1}{4}Br)^{-\frac{1}{6}}, \tag{3.1}$$

and

$$x_c = \ln(\tfrac{1}{8}\Lambda G^3AE)^{-1}, \tag{3.2}$$

where

$$\Lambda = \frac{48\alpha^{\frac{3}{2}}}{[190\pi(1+\tfrac{1}{4}\alpha Br)]^{\frac{1}{2}}}$$

and

$$\alpha = 1 - 2G^{-1}\ln(\tfrac{1}{8}G^3AE)^{-1}.$$

For a given aspect ratio A and speed parameter G the equation

$$x_c = x_s \tag{3.3}$$

may be solved to determine where the short bowl regime changes to a long bowl regime.

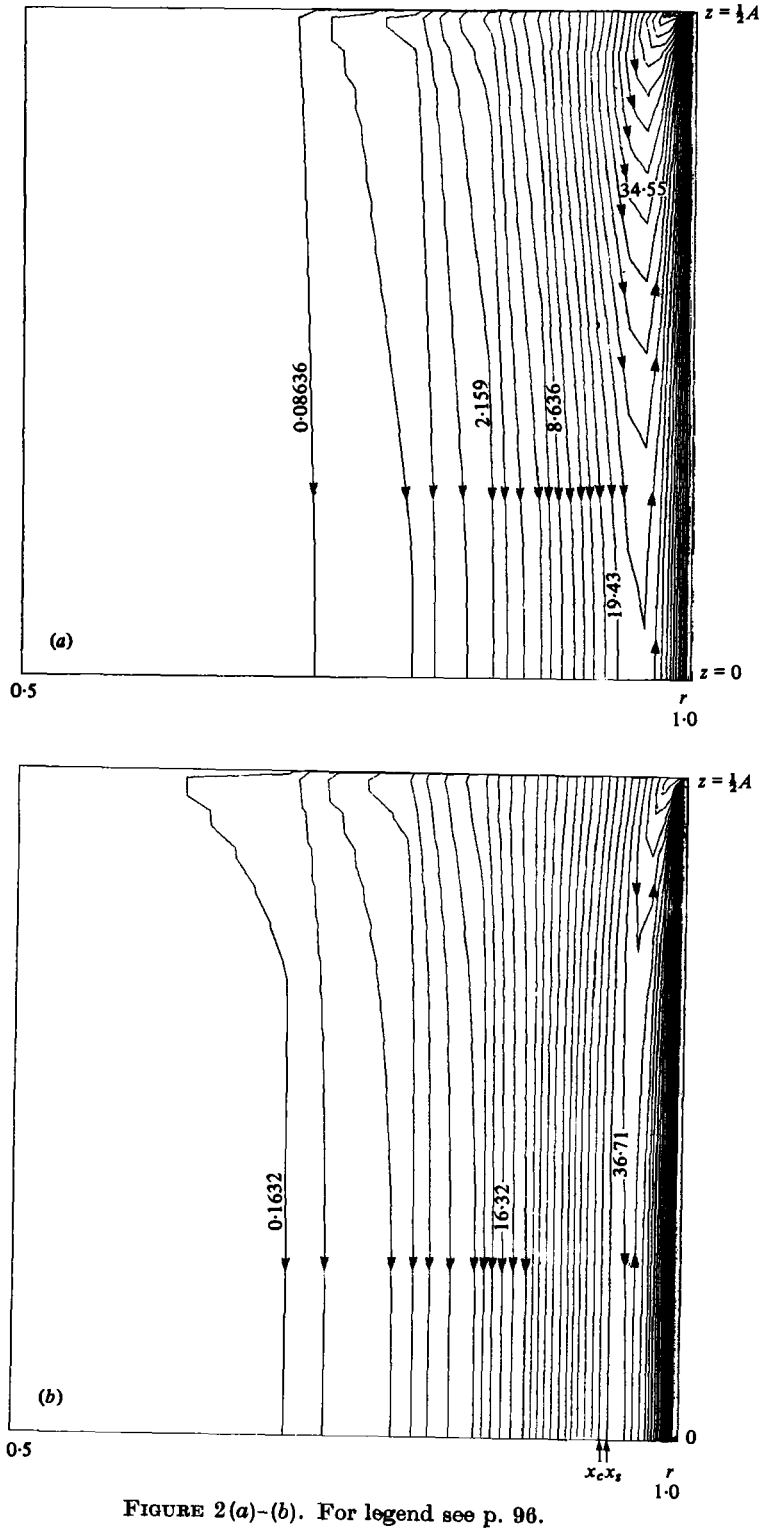

FIGURE 2(*a*)–(*b*). For legend see p. 96.

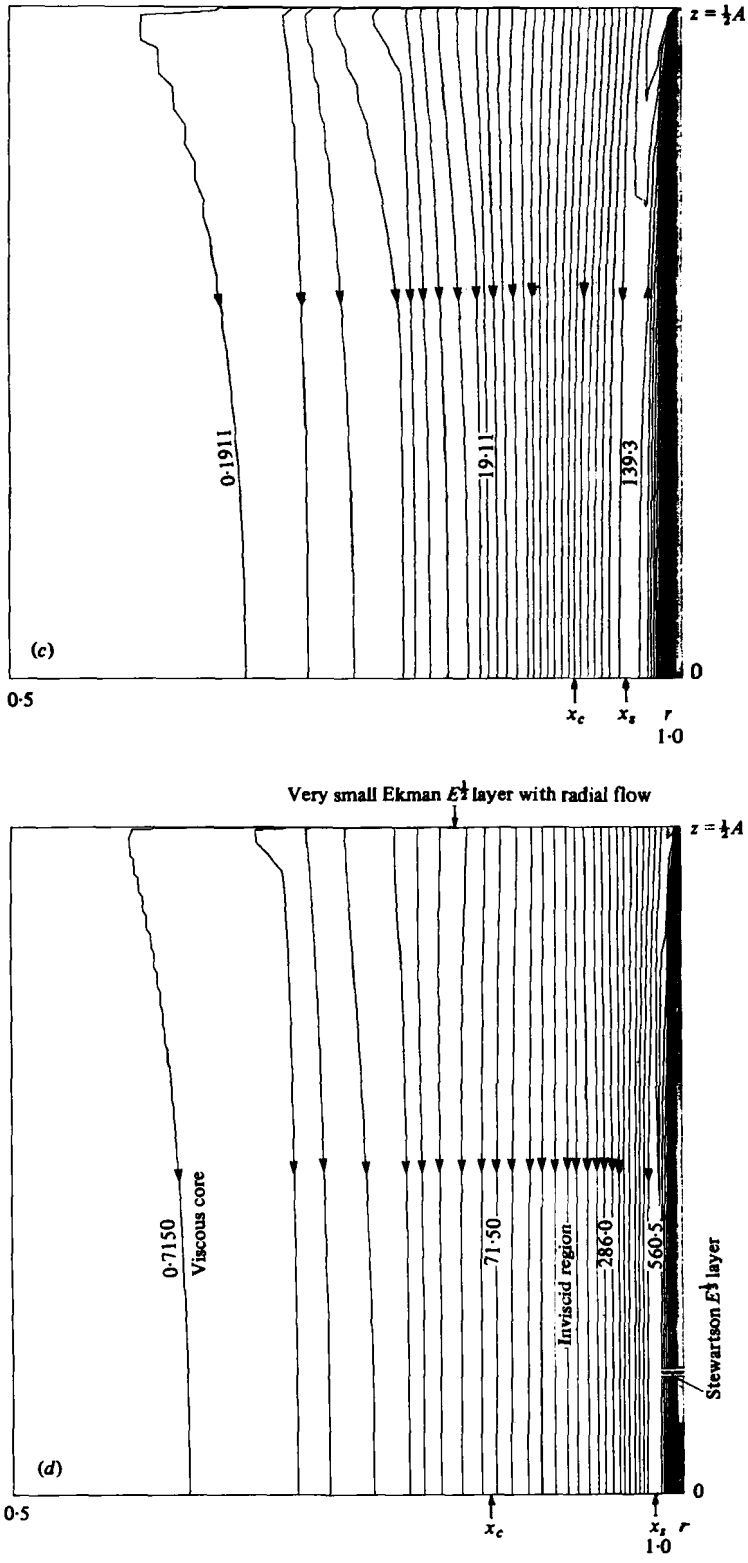

FIGURE 2. Streamlines in the top half of the cylinder due to friction drive $A = 30$, $G = 35$. (*a*) $E = 2{\cdot}7 \times 10^{-6}$, (*b*) $E = 6{\cdot}73 \times 10^{-7}$, (*c*) $E = 3{\cdot}37 \times 10^{-7}$, (*d*) $E = 0{\cdot}56 \times 10^{-7}$; x_c Brouwers core position, x_s Brouwers Stewartson-layer position.

The approximate solutions (3.1) and (3.2) are obtained by assuming that the solution has the form of a quartic polynomial and applying a Pohlhausen technique. As a result of applying this method the boundary layers have well defined thicknesses even though the exact solutions exhibit exponentially damped oscillations. For the side-wall Stewartson layer, the thickness derived from the approximate solution may be identified with the thickness of the 'return layer', i.e. the distance of the first zero of the axial velocity from the side wall or the position of the first local maximum of the stream function. This quantity, the thickness of the return layer, is also easy to identify in the numerical calculation. In the remainder of this section, concerning friction drive, it is therefore assumed that the thickness of the Stewartson layer is that of the return layer, enabling a well-defined Stewartson-layer thickness to be obtained from the numerical results. This is far simpler than using any other definition of the thickness of the layers, such as the momentum thickness, and is consistent with the results of the Pohlhausen techniques. For the purposes of this paper therefore, to examine the range of applicability of the short bowl regime, the assumption is satisfactory and, as will be seen, the errors incurred by this assumption will be small.

Figures 2(*a*)–(*d*) show the computed streamline patterns for friction drive in the top half of the cylinder for $G = 35$, $A = 30$ and a range of Ekman numbers. In each of these figures, 2(*a*)–(*d*), the value of the stream function on the ith contour may be obtained by taking the value indicated on the first contour, the lowest value, and multiplying by i^2. This also applies to the other stream-function contour plots given in this paper.

For this case Brouwers approximate theory predicts, from (3.1) and (3.2), that the long-bowl regime will be valid for $E \gtrsim 8{\cdot}4 \times 10^{-7}$. Numerical results from PACE are in agreement with this result. For $E = 2{\cdot}7 \times 10^{-6}$, figure 2(*a*) PACE predicts strong decay, whereas for $E = 6{\cdot}73 \times 10^{-7}$, figure 2(*b*), there is a noticeable cylinder wall Stewartson layer and a well-defined inviscid region. This inviscid region is characterized by straight vertical streamlines, indicating no radial flow.

As the Ekman number decreases, figures 2(*c*) and 2(*d*), the Stewartson layer becomes narrower and the inviscid region larger. Also marked on these figures are the predicted positions of the edge of the Stewartson layer and viscous core from (3.1) and (3.2). There is reasonable agreement regarding the position of the Stewartson layer except at $E = 6{\cdot}73 \times 10^{-7}$ where axial diffusion is still bound to have some effect.

Examining figures 2(*b*)–(*d*) towards the axis of the cylinder one observes signs of decay where the streamlines are not parallel, the viscous core postulated by Brouwers. The difference between the inviscid flow region and the viscous core is not particularly pronounced for the flow generated by the end wall boundary condition chosen in this study. The position of the viscous core predicted from Brouwers approximate theory also appears to be considerably nearer the cylinder wall than the numerical results indicate. This apparent discrepancy may be understood in terms of the boundary conditions on the stream function assumed in calculating the core position in Brouwers asymptotic theory. The stream function in the inviscid region in Brouwers (1978*a*) results from end wall boundary conditions which have a radial dependence as follows

$$v \propto r e^{\frac{1}{2}x}(1 + \tfrac{1}{4} B r r^2)^{\frac{3}{4}}$$

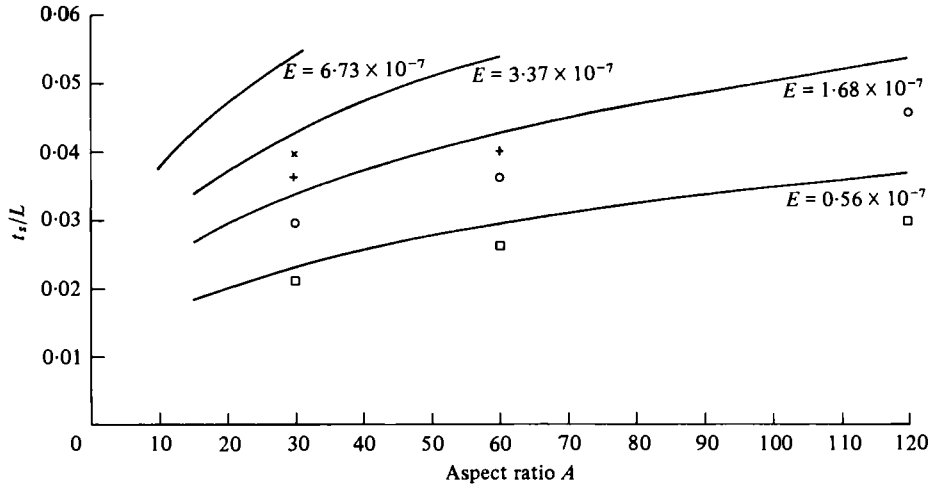

FIGURE 3. Relative thickness of $E^{\frac{1}{2}}$ Stewartson layer at mid-plane, $z = 0$, i.e. t_s/L, as a function of aspect ratio A, $G = 35$. ——, Brouwers; ×, $E = 6.73 \times 10^{-7}$; +, $E = 3.37 \times 10^{-7}$; ○, $E = 1{\cdot}61 \times 10^{-7}$; □, $E = 0{\cdot}56 \times 10^{-7}$. For relative thickness $\gtrsim 0{\cdot}055$ no Stewartson-layer thickness can be defined for $G = 35$.

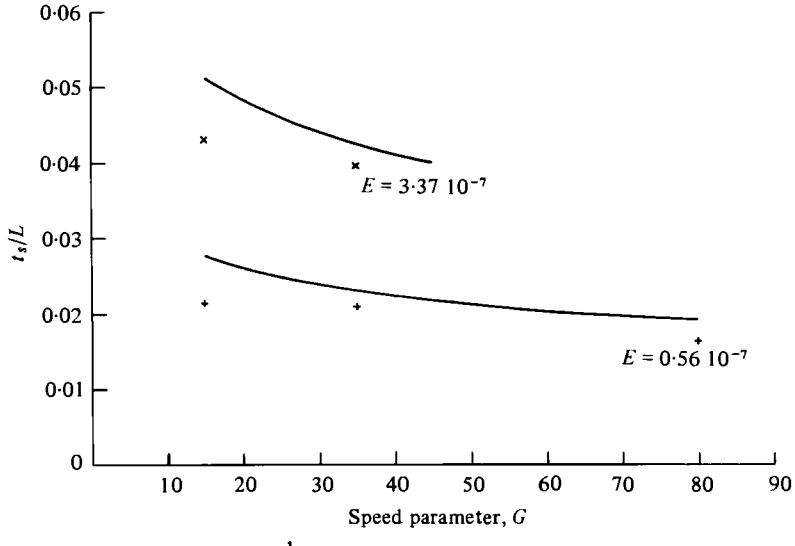

FIGURE 4. Relative thickness of $E^{\frac{1}{2}}$ Stewartson layer at mid-plane, $z = 0$, i.e. t_s/L as a function of speed parameter G, $A = 30$. ——, Brouwers; +, $E = 0{\cdot}56 \times 10^{-7}$; ×, $E = 3{\cdot}37 \times 10^{-7}$.

whereas the inviscid region stream function in the present study arises from $v \propto r$ at the end wall boundary. Defining a stream function by

$$\psi = \frac{-1}{\mu\delta} L \int_0^r \rho q_z^* \, r \, dr$$

the present boundary conditions result in

$$\psi = \tfrac{1}{4}(Ee^x)^{-\frac{1}{2}} r^2 \{1 + \tfrac{1}{4} Br\, r^2\}^{-\frac{3}{4}} \tag{3.4}$$

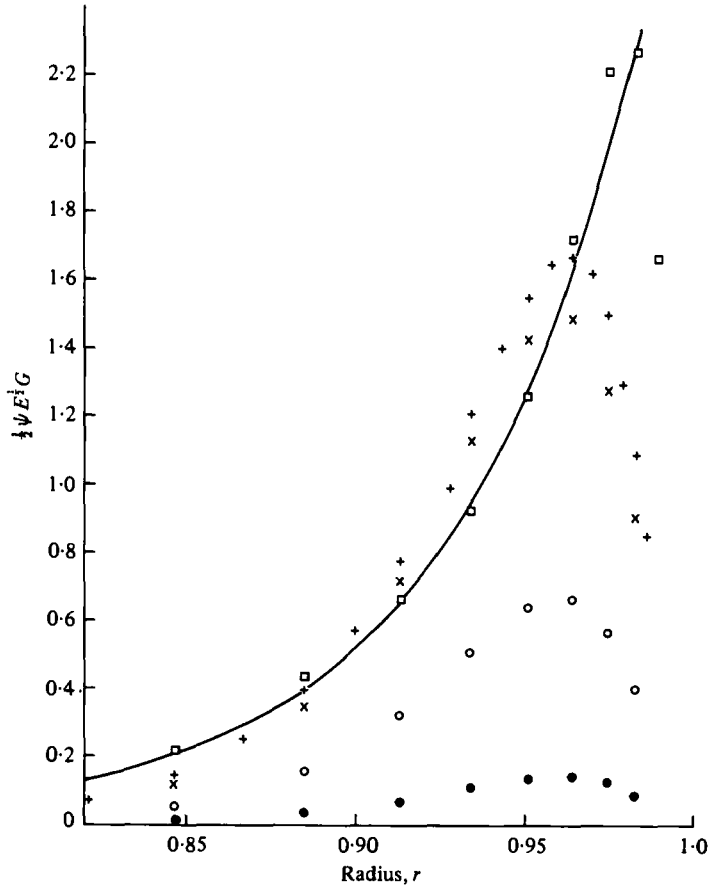

FIGURE 5. Stream function $\times \frac{1}{2}GE^{\frac{1}{2}}$ as a function of radius at mid-plane, $z = 0$ for case $A = 30$, $G = 35$. ——, Inviscid flow from asymptotic theory. ●, $E = 5{\cdot}4 \times 10^{-6}$; ○, $E = 2{\cdot}7 \times 10^{-6}$; ×, $E = 6{\cdot}73 \times 10^{-7}$; +, $E = 3{\cdot}37 \times 10^{-7}$; □, $E = 0{\cdot}56 \times 10^{-7}$.

whereas the stream function based on the assumption of Brouwers would be $\propto r^2$. If the inviscid region stream function related to the present boundary condition were substituted into Brouwers asymptotic analysis, the core position would move towards the axis of rotation, as observed numerically. It is not possible to estimate precisely the core position from the numerical results for this boundary condition, since there is insufficient resolution in the central region to pick up the small difference between the results from the numerical solutions and (3.4). Therefore the best means of identifying the position of the viscous core from the numerical calculations occurs when the core touches the side-wall Stewartson layer and no inviscid region is found.

Figures 2(*a*)–(*d*) also indicate the size of the Ekman $E^{\frac{1}{2}}$ layers on the end walls. The layers are not visible on the graphical scale except near the left-hand edge where the layer is beginning to thicken appreciably. The figures also show how appropriate the term 'Ekman suction' is for the effect of the end-wall layer upon the inviscid region.

Figure 3 shows the effect of varying the aspect ratio upon the thickness of the Stewartson layer. For $G = 35$ and a relative thickness $\gtrsim 0{\cdot}055$ the simple theory of

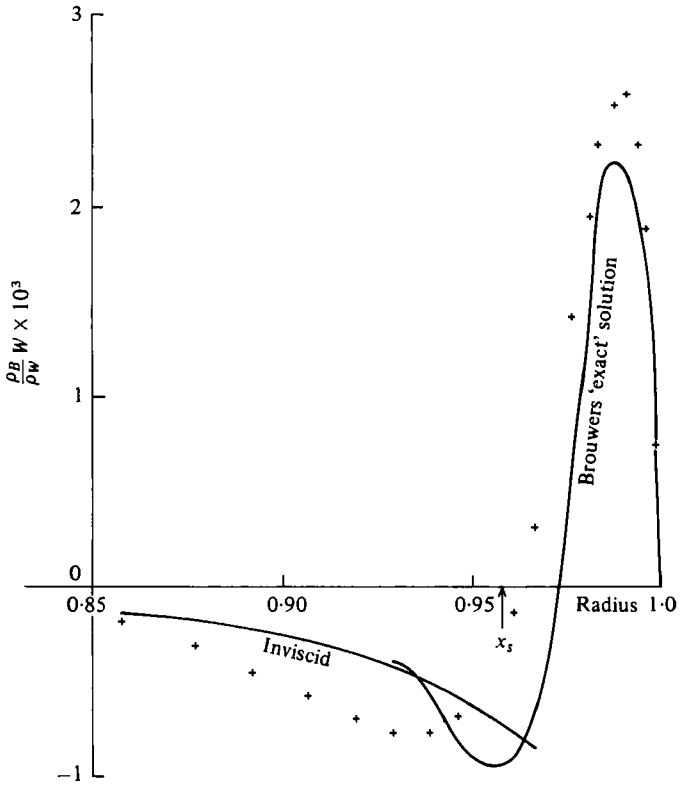

FIGURE 6. Axial velocity in Stewartson layer, $G = 35$, $A = 30$, $E = 3{\cdot}37 \times 10^{-7}$, $z = 0$. +, PACE 30×48 grid; x_s, Brouwers return-layer position from Pohlhausen theory.

Brouwers, from (3.1)–(3.3), predicts that the viscous core meets the Stewartson layer and no inviscid region is to be found. This observation is consistent with the numerical results of PACE.

Figure 4 shows the effect of varying the speed parameter on the thickness of the Stewartson layer. As the speed parameter increases the thickness of the Stewartson layer decreases. It should also be remembered that for a given Ekman number and aspect ratio, increasing the speed parameter results in the core position moving towards the cylinder wall more rapidly than the Stewartson-layer thickness decreases. In extreme cases, increasing speed parameter can again result in the disappearance of the inviscid region. This is illustrated by the case, $E = 3{\cdot}37 \times 10^{-7}$ and $G = 80$, where both asymptotic theory and PACE predict that there is no inviscid region

In both figures 3 and 4 the agreement between the calculations and asymptotic results on the extent of the short bowl regime are good, over a wide range of the parameter values, although the calculations consistently under predict the analytical estimate (3.1) based on Brouwers (1978*a*). It should also be borne in mind that while the differences look appreciable on the figures, the differences in layer thickness are only of the order of 1 % relative to the cylinder radius.

The magnitude of the stream function in the inviscid region can be calculated from the asymptotic theory and for the present boundary conditions on the cylinder end walls is given by (3.4) as a function of radius and is shown in figure 5. Also plotted on

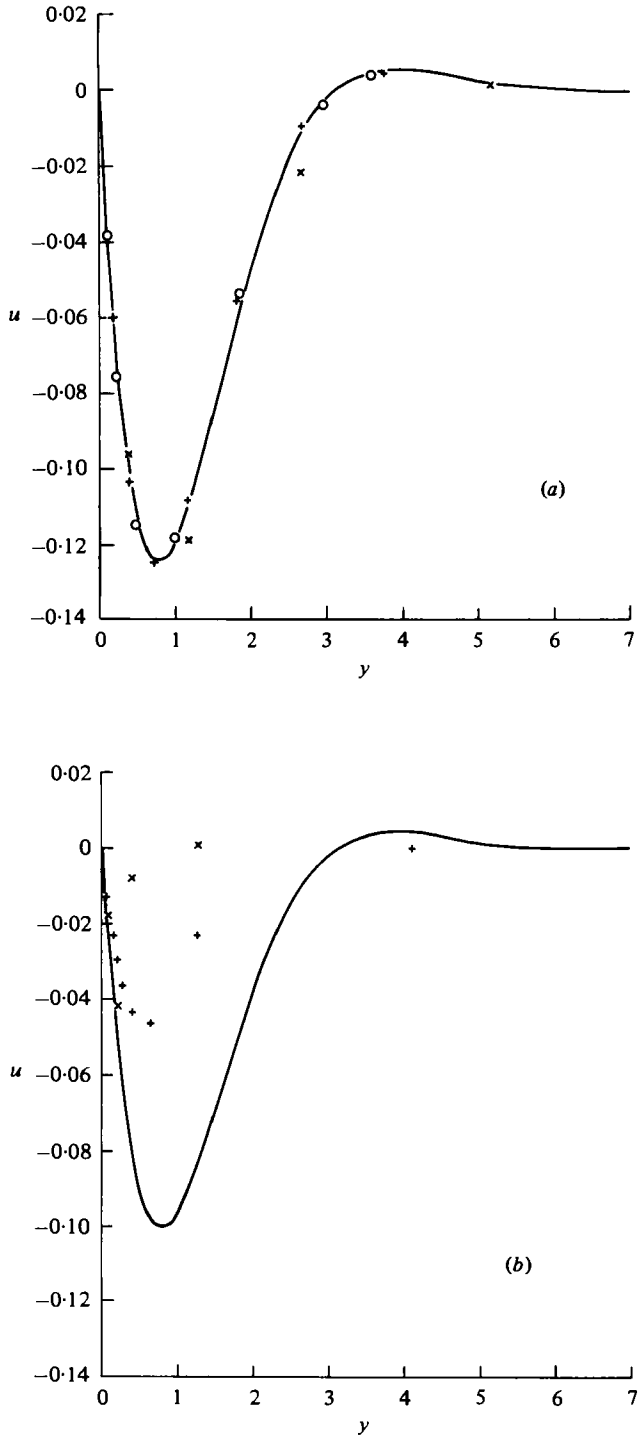

FIGURE 7. Comparison of radial velocity in the Ekman layer, $A = 30$, $G = 35$. ——, Asymptotic theory; ×, $E = 3{\cdot}37 \times 10^{-7}$, 15×24 grid; +, $E = 3{\cdot}37 \times 10^{-7}$, 30×48 grid; ○, $E = 0{\cdot}56 \times 10^{-7}$, 15×48 grid. (*a*) $r = 0{\cdot}964$, (*b*) $r = 0{\cdot}702$.

figure 5 are the computed results from PACE at $z = 0$ for the case $A = 30$, $G = 35$ as a function of Ekman number. At high Ekman numbers there is no evidence of an inviscid region and the effects of axial decay are important.

As a check upon the validity of (3.1) for the extent of the return layer, a comparison has been made in figure 6 between Brouwers' exact series solution for the Stewartson-layer equations, and the numerical results from PACE for the axial mass flow in the mid-plane $z = 0$. Also indicated is the thickness of the return layer, x_s, from (3.1). The agreement between the numerical results and the exact Stewartson-layer solution is reasonable, although the exact solution under predicts the thickness of the return layer. The Pohlhausen solution, on the other hand, gives a better estimate of the position of the return layer. This corresponds roughly in position to the minimum point in the exact solution. There is also a mismatch between the inviscid flow solutions and the exact boundary-layer solution. This is almost certainly due to the assumption made by Brouwers and others that the density within the Stewartson layer does not change appreciably, i.e. $e^x \sim 1$. There is, therefore, ambiguity in comparing results derived from Brouwers' exact solution for his definition of the stream function, to the definition used here, since the non-dimensional density, e^x, is used in the conversion.

Durivault & Louvet (1976), and Bark & Bark (1976) have considered the effect of varying density in the Stewartson layers. Their numerical solutions of the Stewartson layer equations show that the layers are roughly a third thicker than when the density variations are ignored. Their observation is in accord with the results presented in figure 6. For the purpose of estimating the extent of the long bowl regime however this is a fairly small effect. For example, in the cases considered in this paper where an inviscid region may be found it would increase the thickness of the Stewartson layer, relative to the cylinder radius, by at most 3 %.

Analytical solutions for the flow in the Eckman layer have been derived independently by several authors, e.g. Sakurai & Matsuda (1974), Nakayama & Usui (1974), Brouwers (1976). The form for the radial velocity in the layer is given by

$$u = -\tfrac{1}{2}r(1 + 0{\cdot}25Br\,r^2)^{-\frac{1}{2}}\,e^{-y}\sin y \tag{3.5}$$

where $y = (1 + 0{\cdot}25Br\,r^2)^{\frac{1}{4}}\,A(Ee^{\frac{1}{2}G(1-r^2)})^{-\frac{1}{2}}(z - \frac{1}{2}A)$. The radial velocity therefore has the form of a rapidly damped sine wave, the thickness of the layer increasing as r decreases. The radial velocity profile is sketched at one radius in figure 7 (a), together with some numerical results. The agreement is remarkable, demonstrating the ability of the numerical technique to handle the very thin boundary layers which are present. For the Ekman layer considered, the first peak on the radial velocity profile is positioned at about 0·005 % of the height of the computational domain, $\frac{1}{2}A$, away from end wall, whilst the second peak is about 0·04 %. Similar agreement is found at the same radius for cases where the flow decays everywhere, e.g. for $E = 2{\cdot}7 \times 10^{-6}$, and so are not reproduced here.

Brouwers (1978b) also shows that the Ekman layer equations are valid only for $x \ll \ln E^{*-1}$ and for $x \sim \ln E^{*-1}$ all terms of the original equations are important. Figure 7 (b) shows the computed and asymptotic radial velocity profile in the end-wall boundary layer much nearer to the axis than in figure 7 (a). For this case $x = 8{\cdot}87$ and $\ln E^{*-1} = 8{\cdot}2$, so that $x \sim \ln E^{*-1}$. The figure shows that the numerical results are no longer in agreement with the asymptotic solution (3.4) for the Ekman layer. Whilst the accuracy of the numerical results at this radius is not as good as in figure 7 (a) due

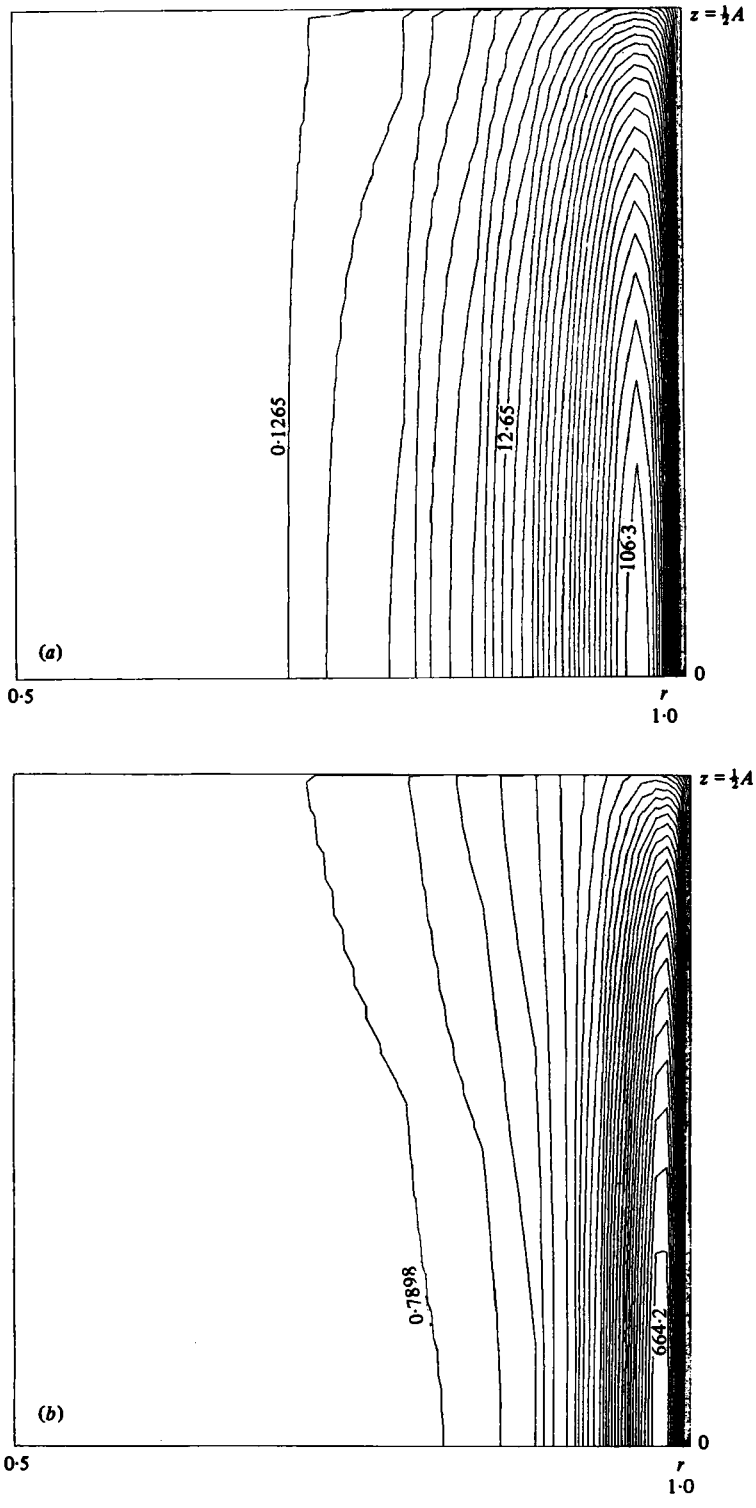

FIGURE 8 (*a*, *b*). For legend see p. 104.

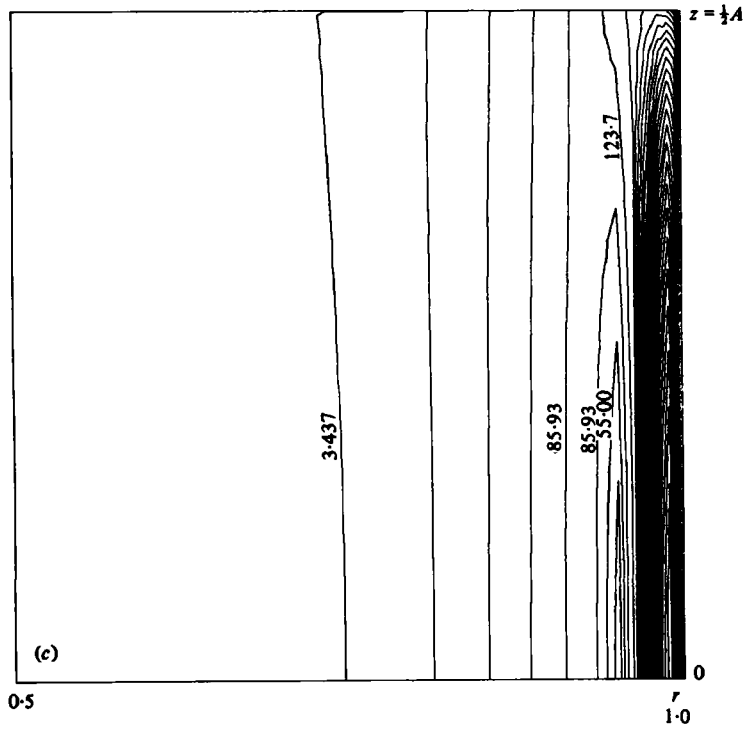

FIGURE 8. Streamlines in the top half of the cylinder due to linear thermal drive, $A = 30$, $G = 35$. (*a*) $E = 2{\cdot}7 \times 10^{-6}$, (*b*) $E = 3{\cdot}37 \times 10^{-7}$, (*c*) $E = 0{\cdot}56 \times 10^{-7}$.

to the much larger radial mesh increments, these results indicate that the neglected radial diffusion terms in the Ekman-layer equations may now be important.

Viscous effects will also be important for the case when the two Ekman layers touch. As these layers grow in extent towards the axis the viscous region in this case will first appear near the axis, giving rise to another type of viscous core. For the aspect ratios considered in this paper, this phenomenon does not occur. This is well illustrated by the results of figure 4 since for a constant Ekman number the long bowl regime occurs as the aspect ratio increases, not decreases.

(*b*) *Linear thermal profile*

For a linearly varying cylinder-wall temperature boundary condition, the $E^{\frac{1}{3}}$ Stewartson layer takes a completely different form. The asymptotic theories predict that instead of simply rechannelling the inviscid flow, there is substantial recirculation within the Stewartson layer and that it is much thicker than that for the friction drive, e.g. Durivault & Louvet (1976), Nakayama & Usui (1974), Sakurai & Matsuda (1974), Mikami (1973) and Brouwers (1976). Figures 8(*a*)–(*c*) show the computed stream function contours for three cases. In the first case there is no inviscid region present as the viscous core fills the machine. In the other two cases an inviscid region is predicted by the asymptotic theory for friction drive, however it is now very difficult to judge the extent of the Stewartson layer from the numerical calculations. At the lowest Ekman number, in figure 8(*c*), a second recirculation region is observed within the

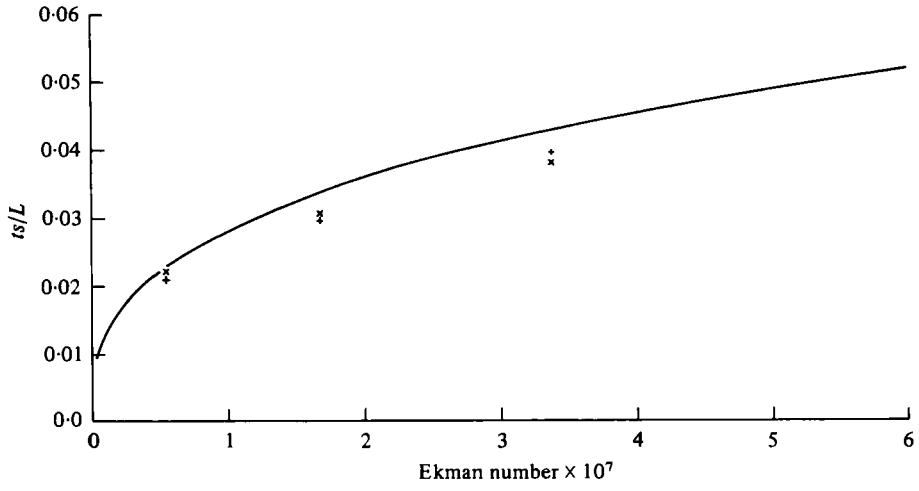

FIGURE 9. Relative thickness of the $E^{\frac{1}{3}}$ Stewartson layer at the mid-plane, $z = 0$, as a function of Ekman number, $A = 30$, $G = 35$. ——, Brouwers; +, numerical calculation for friction drive; ×, return-layer thickness/0·565, linear temperature drive.

Stewartson layer. This is predicted by the asymptotic theories, since the flow profile within the layer is found to have exponentially damped oscillations.

The flow in the end-wall Ekman layers is generated by the boundary conditions on the function $\chi = v/r - \frac{1}{2}T$, thus the asymptotic Ekman-layer solutions are identical to those for friction drive, except for a factor 2. The agreement for the radial velocity in the Ekman layer between the asymptotic and numerical predictions is similar to that found in figure 7. As the behaviour of these Ekman-layer solutions also governs the inviscid flow in the interior the inviscid stream function is given by half equation (3.5).

The stream function in the interior due to the Ekman-layer flow is therefore $\propto E^{-\frac{1}{2}}$. The asymptotic analyses however, e.g. Brouwers (1976) show that the magnitude of the stream-function maximum for the Stewartson-layer solutions arising from this boundary condition is approximately $\propto E^{-1}$. This dependence is observed in the calculations. The recirculating flow in the Stewartson layer is therefore much stronger for small Ekman numbers than the flow recirculating in the interior from one Ekman layer to the other. This also explains why the second recirculating region in the Stewartson-layer solutions is only visible in figure 8(*c*). For higher Ekman numbers this recirculation is swamped by the inviscid flow solution and it is only at very low Ekman numbers that this second recirculating region is visible. Detailed comparison of the inviscid flow solution with the results from PACE in a similar fashion to that in figure 5, shows that axial decay is important for the first two cases considered in figure 8, and a well-defined inviscid region is to be found only in figure 8(*c*), i.e. $E = 0{\cdot}56 \times 10^{-7}$. It is apparent that the thicker Stewartson layer associated with the linear thermal drive touches the viscous core at lower Ekman numbers than for friction drive, consequently viscous effects are more important for a linear thermal drive than for friction drive over the parameter ranges considered.

The asymptotic analyses are now little help in deriving a simple expression for the extent of the Stewartson layer. Since the Stewartson layer is so thick, there are

appreciable variations in the rigid body density e^z across the layer and the approximation $e^z = 1$ is not as good as for a friction drive. For example, for the case of figure 8(*c*), e^z is about 0·1 near the edge of the Stewartson layer. The Stewartson layer equations without the assumption of constant density, are not amenable to easy analytic solution and numerical solutions are generally obtained. Since this is non-trivial we have not carried out any comparison with the results of the asymptotic predictions for the flow within the Stewartson layer. Louvet & Cortet (1979) have conducted a comparison between numerical solutions of the full-linearized equations and the numerical solution of the Stewartson layer equations (including the variation of density) in the short bowl regime and found good agreement between the two treatments.

A simple formula may however be obtained for the thickness of the 'return' layer, the distance between the cylinder wall and the first maximum of the stream function. Brouwers (1976) finds that the ratio of these two distances is approximately 0·565. In figure 9, the analytic thickness of the Stewartson layer for friction drive given by (3.1) is graphed for $Z = 0$, $G = 3{\cdot}5$ and $A = 30$, together with the computed thickness for friction drive and the computed returns layer thickness for thermal drive divided by 0·565. Once again agreement is good.

4. Conclusions

The primary conclusion to be drawn from this work is that the predictions from the asymptotic theories of Brouwers regarding the influence of the viscous core are in good agreement with the numerical results. In particular the Pohlhausen solutions for a friction drive provide simple estimates of the extent of the core and the side-wall Stewartson layer and, despite a different end-wall boundary condition, give a good indication of the nature of the flow. It is important therefore that other asymptotic analyses based on the modified incompressible or short bowl approach correctly take into account the effects of the viscous core, particularly if the parameters are such that the core touches either of the Stewartson $E^{\frac{1}{3}}$, or for non-antisymmetric conditions, the much thicker $E^{\frac{1}{4}}$ layer.

It is difficult to apply the analytic asymptotic theories to more complex boundary conditions. However the theories do still provide a useful guide to the nature of the solutions of the linear equations and their underlying physics.

This work was performed under contract for BNFL and Urenco/Centec.

REFERENCES

Bark, F. H. & Bark, T. H. 1976 Vertical boundary layers in a rotating gas. *J. Fluid Mech.* **78**, 749.

Brouwers, J. J. H. 1976 On the motion of a compressible fluid in a rotating cylinder. Ph.D. thesis, Twente Institute of Technology, Enschede, The Netherlands.

Brouwers, J. J. H. 1978*a* On the compressible flow in a gas centrifuge and its effect on the maximum separative power. *Nuc. Tech.* **39**, 311.

Brouwers, J. J. H. 1978*b* On compressible flow in a rotating cylinder. *J. Eng. Maths.* **12**, 265.

Duff, I. S. 1977 MA28A – A set of Fortran subroutines for sparse unsymmetric linear equations. AERE-R. 8730.

DURIVAULT, J. & LOUVET, P. 1976 Étude de la couche de Stewartson compressible dans une centrifugeuse à contrecourant thermique. *C.R. Acad. Sci. Séance* **283**, 79.

KÁLNAY DE RIVAS, E. 1972 On the use of non-uniform grids in finite difference equations. *J. Comp. Phys.* **10**, 202.

LOUVET, P. & CORTET, C. 1979 Discussion of various flow calculation methods in high-speed centrifuges. *Proc. 3rd Workshop on Gases in Strong Rotation* (ed. G. B. Scuricini). Rome: CNEN.

MATSUDA, T., HASHIMOTO, K., TAKEDA, H. 1976 Thermally driven flow in a gas centrifuge with insulated side walls. *J. Fluid Mech.* **73**, 389.

MIKAMI, H. 1973 Thermally induced flow in a gas centrifuge. *J. Nucl. Sci. Tech.* **10**, 580.

NAKAYAMA, W. & USUI, S. 1974 Flow in a rotating cylinder of a gas centrifuge. *J. Nucl. Sci. Tech.* **11**, 242.

ORSAG, S. A. & ISRAELI, M. 1974 Numerical simulation of viscous incompressible flows. *Ann. Rev. Fluid Mech.* **6**, 281.

PARKER, H. M. & MAYO, T. T. 1963 Counter-current flow in a semi-infinite gas centrifuge. Preliminary results. *Res. Lab. Engng Sci., Univ. Virginia, Rep.* no. E1-4422-279-630.

RÄTZ, E. 1978 Uranium isotope separation in the gas centrifuge. *Von Karman Institute for Fluid Dynamics.* Lecture series 1978 Rhode St Genèse, Belgium.

ROACHE, P. J. 1972 *Computational Fluid Dynamics.* Albuquerque. New Mexico: Hermosa.

SAKURAI, T. & MATSUDA, T. 1974 Gas dynamics of a centrifugal machine. *J. Fluid Mech.* **62**, 727.

SOUBBARAMAYER 1979 Centrifugation in Uranium Enrichment. *Topics in Appl. Phys.* vol. 35 (ed. S. Villani). Springer.

STEENBECK, M. 1958 Erzeugung einer selbstkaskadierenden Axialströmung in einer langen Ultrazentrifuge zur Isotopentrennung. *Kernenergie* **1**, 921.

STEWARTSON, K. 1957 On almost rigid rotations. *J. Fluid Mech.* **3**, 17.